AUT Journal of Mechanical Engineering

AUT J. Mech. Eng., 7(2) (2023) 185-198
DOI: 10.22060/AJME.2023.22354.6062

Numerical Investigation Of The Best Wind Turbine Shroud Flange Curvature For Maximum Wind Power Extraction

Ali Niknahad, Abdolamir Bak-Khoshnevis*

Faculty of Mechanical Engineering, Hakim Sabzevari University, Sabzevar, Iran

ABSTRACT: In today's world, net zero energy buildings are growing and developing. These buildings generally supply their energy needs from renewable sources such as wind. Unfortunately, in urban areas, the quality of the passing wind is low and it is not able to create the necessary force for the proper rotation of turbines. To overcome this problem, it is necessary to use a tool that can speed up the flow like a shroud. In the present work, a vertical straight flange is considered at the end of the shroud. The points in the middle of the flange height move to the end of the shroud with a very small interval and create different curves. By using this procedure, a flange with an optimal curve that is able to create the highest mean velocity of air passing through the shroud will be obtained. The results show a significant increase in mean velocity, which has been confirmed by studies of turbulent kinetic energy behind the turbine shroud. Based on the results of a three-dimensional simulation, it is concluded that in the turbine section, a mean velocity increase of 20% can be achieved, which is the first time that using an aerodynamic cross-section for the flange of the shroud and optimizing it has achieved such a great increase in air mean velocity along wind turbine shroud.

Review History:

Received: Apr. 26, 2023
Revised: Sep. 08, 2023
Accepted: Sep. 09, 2023
Available Online: Oct. 02, 2023

Keywords:

Shroud
Flange
Wind turbine
CFD

1- Introduction

The use of clean energy guarantees the health of the planet and future generations. The use of renewable energy, in addition to reducing pollution from fossil fuels to generate power, will preserve fossil fuel reserves for the future. In the meantime, wind turbines and related equipment have a wide position, but it is necessary to pay attention to the fact that they must be built with the best design and then reach the consumers. The use of optimal aerodynamic shapes has always resulted in lower costs and higher efficiency. Therefore, aerodynamic optimization is very necessary for the construction of wind turbine shrouds, which are an integral part of urban wind turbines. In the following, past works related to wind and water turbine shrouds will be examined to create a necessary background for the present work.

Han et.al [1] designed wind turbines with shroud and lobed ejectors for efficient utilization of low-grade wind energy. The performance of the planned wind turbine was assessed. Simulation outcomes showed that the wind energy operation efficacy of the planned wind turbine increased to 66-73% at low wind speeds extending from 2 to 6 m/s. The shroud and lobed ejector construction in the back of the planned wind turbine formed such an effect that the pressure at the wind turbine exit was reduced and as a result, the turbine power output was increased by 240%.

Dilimulati et.al [2] investigated a case study of shrouded diffuser casing for turbines for urban applications. The diffuser shroud mechanism can draw the airflow over buildings to guide and accelerate the airflow inside. The CFD result approves the functionality of the fluid machine to take advantage of the airflow over buildings for wind power generation. Power amplification using diffusers and shrouded edges around conventional wind turbines shows a noteworthy power coefficient increase.

Shahsavarifard and Bibeau [3] studied the performance characteristics of shrouded horizontal axis hydrokinetic turbines in yawed conditions. Assessing hydrokinetic turbines in yaw conditions contributes to approximating turbine performance, power constancy, and power carried to the network. Water tunnel tests show performance reduction using three strategies: no shroud, a convergent-divergent shroud, and a diffuser shroud. The convergent–divergent shroud shows less performance loss compared to the other two strategies. The maximum decrease in performance of the model turbine with the shroud is 6% on average, which is 17% less than the power decrease of the unshrouded turbine. The shroud retains the functional range of the turbine unaffected.

Ilhan et.al [4] stated that determining the flow formation in the flanged diffuser shrouding considered to be used for a wind turbine, plays a fundamental function in improving efficiency in small-scale wind turbine technology. The dimensionless velocity at downstream and up radial regions

*Corresponding author's email: khoshnevis@hsu.ac.ir

as well as at the flange downstream of the curved type wind turbine shroud, exposed that consequential velocity was amplified by a factor of 1.5. This enhancement of the wind velocity will result in the wind energy interacting with the rotor blades being improved by 3.38 times.

Lipian et.al [5] investigated experimentally a shrouded and twin-rotor wind turbine system for small wind turbine augmentation. The goal was to compare the performance of the same rotor in various configurations. While boosting the wind turbine functionality, shrouding growths meaningfully the rotor loading. A cure for it is the application of another rotor. Although it offers an efficiency increase (11-13% for the unshrouded, 4-5% for the shrouded turbine), it permits loads to be spread more uniformly on turbines. The highest power coefficient decreases meaningfully alongside the wind velocity. This is as a result of rather low Reynolds number. After using shrouding, an around double growth in the first wind turbine power coefficient has been seen at the identical wind velocity.

Lipian et.al [6] investigated numerically shrouded and twin-rotor wind turbine systems for small wind turbine augmentation. The model was used in a universal investigation of the stream nature in the rotor plane, markedly velocity fields. There is a worthy qualitative relationship between DAWT and CRSR arrangements. A tip loss modification for BET-based models was expressed. It corrects the circulation distribution in the wake by changing the number of blades. The investigation displays how the mounting pole of a second wind turbine affects the rotor functionality. The negative effect of this phenomenon is very strong and chiefly restricted to the section in the pole's immediate wake. The velocity fields in the upper half of the rotor stay regularly circumferentially similar.

Leloudas et.al [7] investigated a robust methodology for the design optimization of diffuser-augmented wind turbine shrouds. Their work shows the development of a modular optimization scheme for the aerodynamic form optimization of diffuser-augmented wind turbine shrouds. The optimization caused a shroud design (denoted as SD1) resulting in a mean-velocity speed-up ratio of 1.9, which is 23% higher than the mean velocity speed-up ratio of the basic strategy, go together with a notable decrease in superficial drag by about 47%.

Keramat Siavash et.al [8] investigated an innovative variable shroud for micro wind turbines. A 370-W small wind turbine was developed which is armed with a manageable nuzzle diffuser duct. The developed duct contains a fixed ring and a two-piece diffuser which can revolve around each other and so the diffuser wall opening will have changed from 0 to 180 degrees. Experimental outcomes display a full raise in power generation and rotor speed by shrouded wind turbines. In the 180-degree diffuser wall opening, the amplification ratio on average is 39.75% while the ratio is 28.5% for a complete diffuser amplified wind turbine. The rotor speed-up ratio is 53 and 74% respectively.

Ohya et.al [9] developed a shrouded wind turbine with a flanged diffuser. Emphasis is placed on placing the flange at the outlet of a diffuser shroud. An extraordinary growth in wind speed of 1.6–2.4 times freestream velocity is obtained. They have examined the best shape of the flanged diffuser to find a greater power production of the shrouded wind turbine. A flanged diffuser-shrouded wind turbine established power amplification by a factor of about 4–5 compared to a bare wind turbine.

Gish et.al [10] evaluated experimentally a shrouded horizontal axis hydrokinetic turbine with pre-swirl stators. By using pre-swirl stators to the shroud, it is possible to change the inlet flow to maximize the net tangential force on the turbine blades and grow power output. Four dissimilar pre-swirl stator arrangements were planned and examined on a shrouded3- bladed turbine. At the lowest Reynolds number, all 4 stator arrangements enhanced the maximum Cp by 5–23% compared to the bare turbine. The stator result was neutral at the intermediate and maximum Reynolds numbers and one arrangement presented an adverse result at the highest Reynolds number.

Rezek et.al [11] presented an optimization study for designing a shrouded turbine diffuser. The consequences have shown that the optimum diffuser achieves a power coefficient of about 118%. This method provides the data for the rotor design procedure and can be used to characterize the beginning characteristics of the entire apparatus based on an optimized pre-design.

Kosasih and Tondelli [12] studied experimentally a shrouded micro-wind turbine. The functionality augmentation is influenced by numerous factors such as the diffuser geometries, blade airfoils, and the wind condition at the mounting site. Straight diffuser, nozzle-diffuser combination, and diffuser-brim combination functionality have been examined. Adding a simple conical diffuser can augment the micro wind turbine coefficient of functionality by about 60%, and 63% by using a nozzle conical diffuser shroud compared to the simple turbine. The diffuser and nozzle-diffuser grow optimum TSR by 33% compared to the simple turbine.

Aranake and Duraisamy [13] optimized the aerodynamics of shrouded wind turbines. An axisymmetric RANS solver is used with an actuator disk model for the examination of shrouded wind turbine flow fields. An effective blade design method that maximizes sectional power generation is established. The optimum result is also assessed using a full 3-D RANS solver. Instead of assessing the forces based on a given blade twist, the blade twist is defined such that the angle of attack of each segment is optimum regarding the local flow angle. A project result that surpassed the Betz limit by a factor of 1.43 based on the maximum shroud area is obtained. Physical considerations can limit the scalability of the turbine to very huge configurations, but shrouded turbines are a good solution at smaller scales.

Werle [14] studied an improved analytical model for airfoil-based shrouded wind turbines. A lower-order model for forecasting the functionality of shrouded wind turbines for a range of shroud airfoil shapes. The accuracy of the method is evaluated using inviscid and viscous computational studies. Great engineering estimates can be obtained by

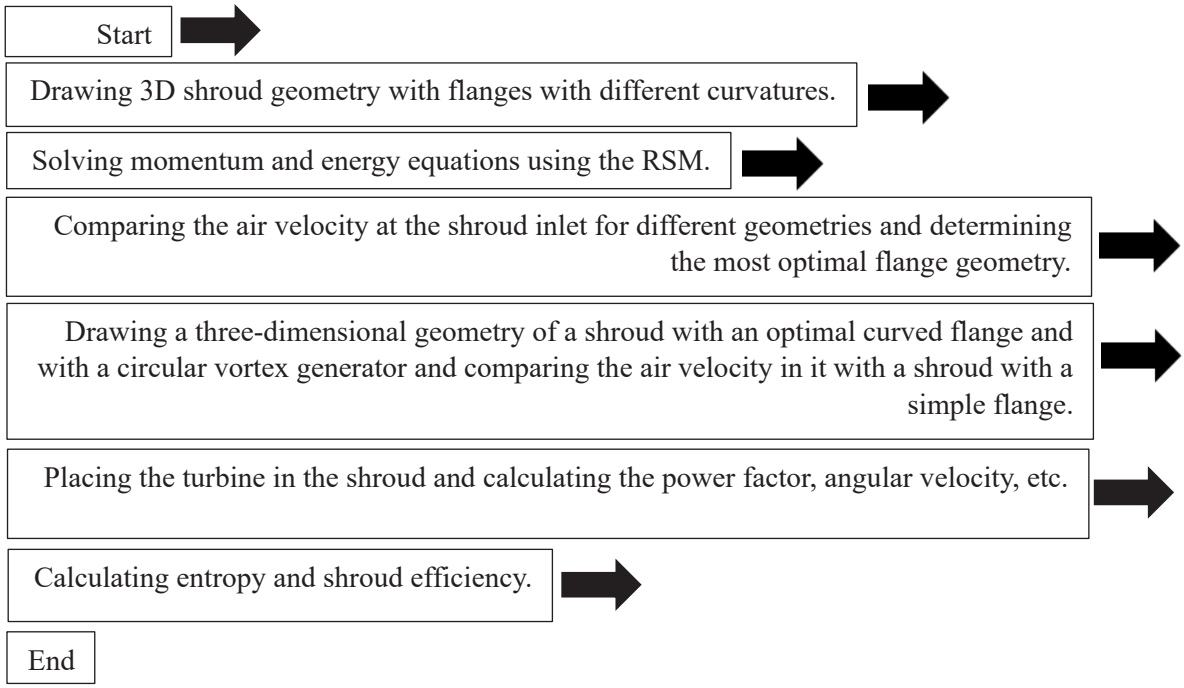

using the algebraic solutions of this technique. To get better results from this model, some aspects of the model must be considered before beginning the shrouded turbine design.

Due to the increasing need of households for energy, newer methods should be used to increase the production capacity of turbines. This need can create a gap that has been tried to fill in the present work. Also, the use of optimization methods, efficient and at the same time simple geometries to increase the power of urban wind turbines is an important matter that has been given special attention in the present work. In the present study, by using two-dimensional optimization of a vertical straight flange installed on an urban wind turbine, an aerodynamic-shaped flange with the ability to create the maximum wind mean velocity passing through the shroud has been obtained. Then the values are confirmed by examining the results of turbulent kinetic energy. Also, with the results obtained from the three-dimensional solution of shrouds with simple and shrouds with optimal flanges, the percentage of increase in mean velocity in the turbine section has been calculated.

2- Methodology

In this project, many wind turbine shroud's flange geometries to find the optimum geometry for catching and accelerating the wing, are investigated. The flow around two-dimensional wind turbine shroud cases is solved by considering the unsteady characteristics of the flow around it. For considering the turbulent nature of the flow field, the RSM turbulent model is found well and used for flow simulation. Finally, the flow field variables in each case are compared to find the optimum wind turbine shroud geometry based on the maximum shroud inlet mean velocity. In this research, Fluent 18.2 software was used as a solver.

2- 1- Governing equations

In this study, the airflow Mach number is below 0.3 and the assumption of incompressibility is valid. Thus the incompressible form of continuity, momentum, and energy equations for turbulent flow are considered. Equations 1 and 2 show the RANS form of continuity and momentum equations, respectively.

$$\frac{\delta \bar{u}_i}{\delta x_i} = 0 \tag{1}$$

$$\frac{\delta \bar{u}_i \bar{u}_j}{\delta x_i} + \frac{1}{\rho}\frac{\delta \bar{p}}{\delta x_i} = \frac{\delta}{\delta x_i}\left(\bar{\tau}_{ij} - \rho\overline{u_i' u_j'}\right) \tag{2}$$

2- 2- Turbulent model

For considering the turbulence nature of the flow field, second-moment closure Reynolds stress model (RSM) turbulence modeling is used. RSM relies on the "Reynolds Stress Transport Equation" and equations 3 to 12 show all employed equations in the corresponding model. The equation for the transport of kinematic Reynolds stress $R_{ij} = u_i' u_j'$ is:

$$\frac{DR_{ij}}{Dx} = D_{ij} + P_{ij} + \prod_{ij} + \Omega_{ij} - \varepsilon_{ij} \tag{3}$$

Production term:

$$P_{ij} = -\left(R_{im} \frac{\partial u_j}{\partial x_m} \right) + R_{im} \frac{\partial u_i}{d x_m} \tag{4}$$

Rapid pressure-strain correlation term:

$$\frac{\prod_{ij}^{R}}{k} = C_2 S_{ij} + C_3 \left(b_{ik} S_{ik} + b_{ik} S_{ik} - \frac{2}{3} b_{mn} S_{mn} \delta_{ij} \right) + C_4 \left(b_{ik} W_{jk} + b_{jk} + W_{ik} \right) \tag{5}$$

$$b_{ij} = \frac{\overline{u_i u_j}}{2k} - \frac{\delta_{ij}}{3} \tag{6}$$

Slow pressure-strain correlation term:

$$\prod_{ij}^{s} = -C_1 \frac{\varepsilon}{k} \left(R_{ij} - \frac{2}{3} k \delta_{ij} \right) - C_2 \left(P_{ij} - \frac{2}{3} P \delta_{ij} \right) \tag{7}$$

Dissipation term:

$$\varepsilon_{ij} = \frac{2}{3} \varepsilon \varepsilon_{ij} or e_{ij} = 0 \tag{8}$$

$$e_{ij} = \frac{\varepsilon_{ij}}{\varepsilon} - \frac{2 \delta_{ij}}{3} \tag{9}$$

Diffusion term:

$$D_{ij} = \frac{\partial}{\partial x_m} \left(\frac{\nu_t}{\sigma_k} \frac{\partial R_{ij}}{\partial x_m} \right) = div \left(\frac{\nu_t}{\sigma_k} \nabla \left(R_{ij} \right) \right) \tag{10}$$

$$\nu_t = C_\mu \frac{k^2}{s}, \sigma_k = 1, C_\mu = -0.09 \tag{11}$$

Rotational term:

$$\Omega_{ij} = -2 \omega_k \left(R_{jm} e_{ikm} + R_{im} e_{jkm} \right) \tag{12}$$

$e_{jkm} = 1$, if i, j, k are in cyclic order and are different. $e_{jkm} = -1$, if i, j, k are in anti-cyclic order and are different. $e_{jkm} = 0$ in case any two indices are the same.

2- 3- Geometry

In the present study, unlike many previous works and based on [10], NACA0006 airfoil has been used in the design of shroud cross-sections in two-dimensional and three-dimensional simulations, which can increase the output power. The length of the airfoil chord is considered to be 450 mm. The diameter of the inlet of the shroud is considered to be 302.24 mm. Also, the length of the shroud based on [9] is obtained using the ratio L/D=1.5. A vertical straight flange is installed at the end of the shroud, which is also known as a simple flange. Also, the value of flange height is obtained based on the relationship h/D=0.25 [9]. As mentioned earlier, the present study aims to find an aerodynamic and optimal shape for the flange. For this purpose, the points located in the middle of the flange height are moved with very small intervals to the end of the shroud and create a special curve at each step. In this way, a wide variety of shapes of the flange are obtained. A schematic of the two-dimensional shroud geometry with straight-vertical flange and flanges whose midpoint of height is shifted 1, 10, 20, and 25 mm to the end of the shroud (δ) (case 1 to case 5) is shown in Figure 1. Also shown in Figure 2 is a three-dimensional schematic of the shroud and flange attached to its end.

2- 4- Boundary conditions and grid generating-mesh independency

The boundary conditions used in this research are an air velocity inlet with a velocity of 15 m/s and a constant pressure outlet with 101000 Pascal. The internal and external body of the shroud also uses the wall boundary condition.

In this section, meshing and examining the mesh independence for two-dimensional and three-dimensional studies are discussed in turn. In this study, the maximum values of mean velocity and turbulent kinetic energy are presented to investigate the mesh independence.

According to the observations from Table 1, the number of optimal grid cells for two and three-dimensional geometries is 602,100 and 3,700,000, respectively. The reason for selecting this number of grid cells is that the changes in flow parameters are less than 0.1%. Figure 3 shows the mesh grids used in 3D simulations based on the results of mesh independency.

In addition to examining the independence of the mesh, the Yplus diagram is also examined. What comes out of Figure 4 is that the amount of Yplus is much less than the unity around the shroud.

2- 5- Numerical method

In this study, the corresponding governing equations are solved numerically with double precision accuracy and a pressure-based algorithm. The unsteady terms in equations are considered and the Semi-Implicit Method for Pressure Linked Equations is selected as the appropriate pressure-velocity coupling. The second-order accuracy for all discretization of governing equations is selected to ensure sufficient accuracy. The convergence criterion is selected 10^{-6} [16] for residuals of equations.

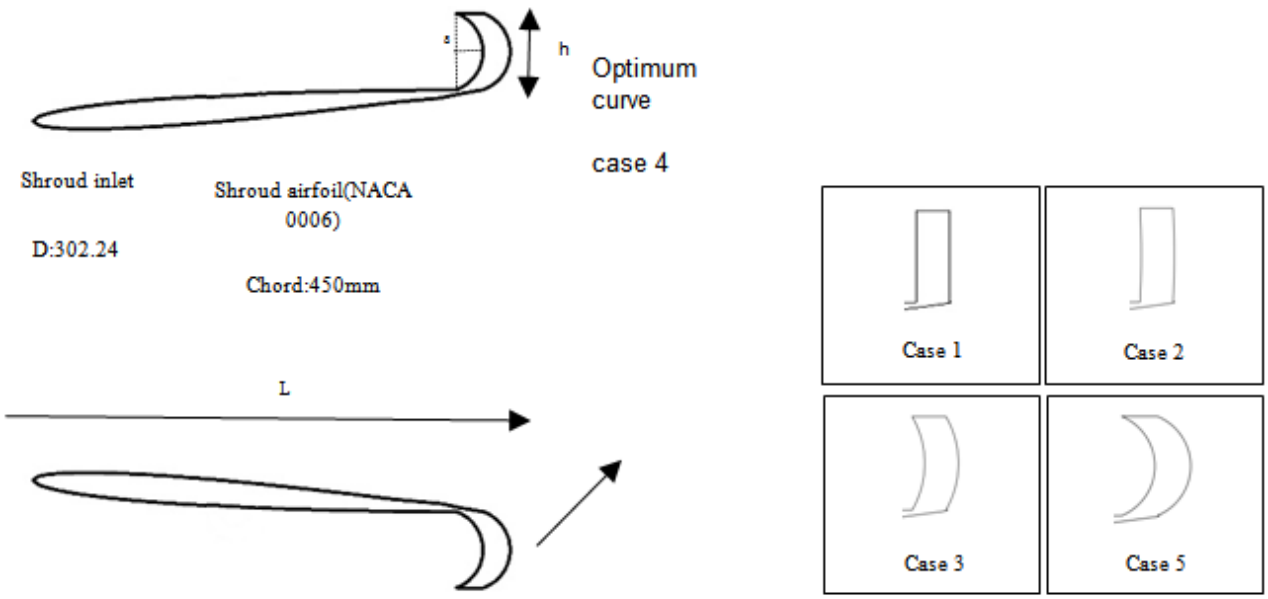

Fig. 1. Base shroud model with a straight vertical and curved flanges

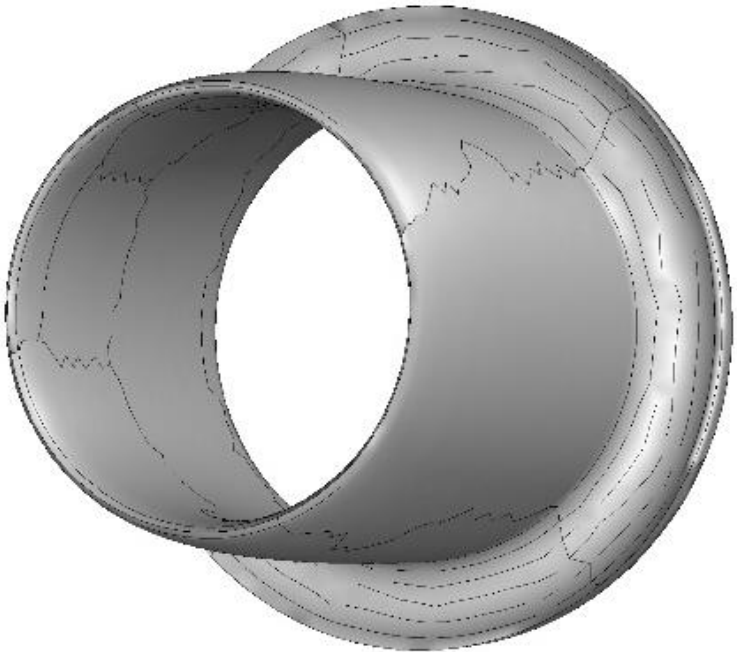

Fig.2. Three-dimensional schematic of the shroud and flange attached to its end

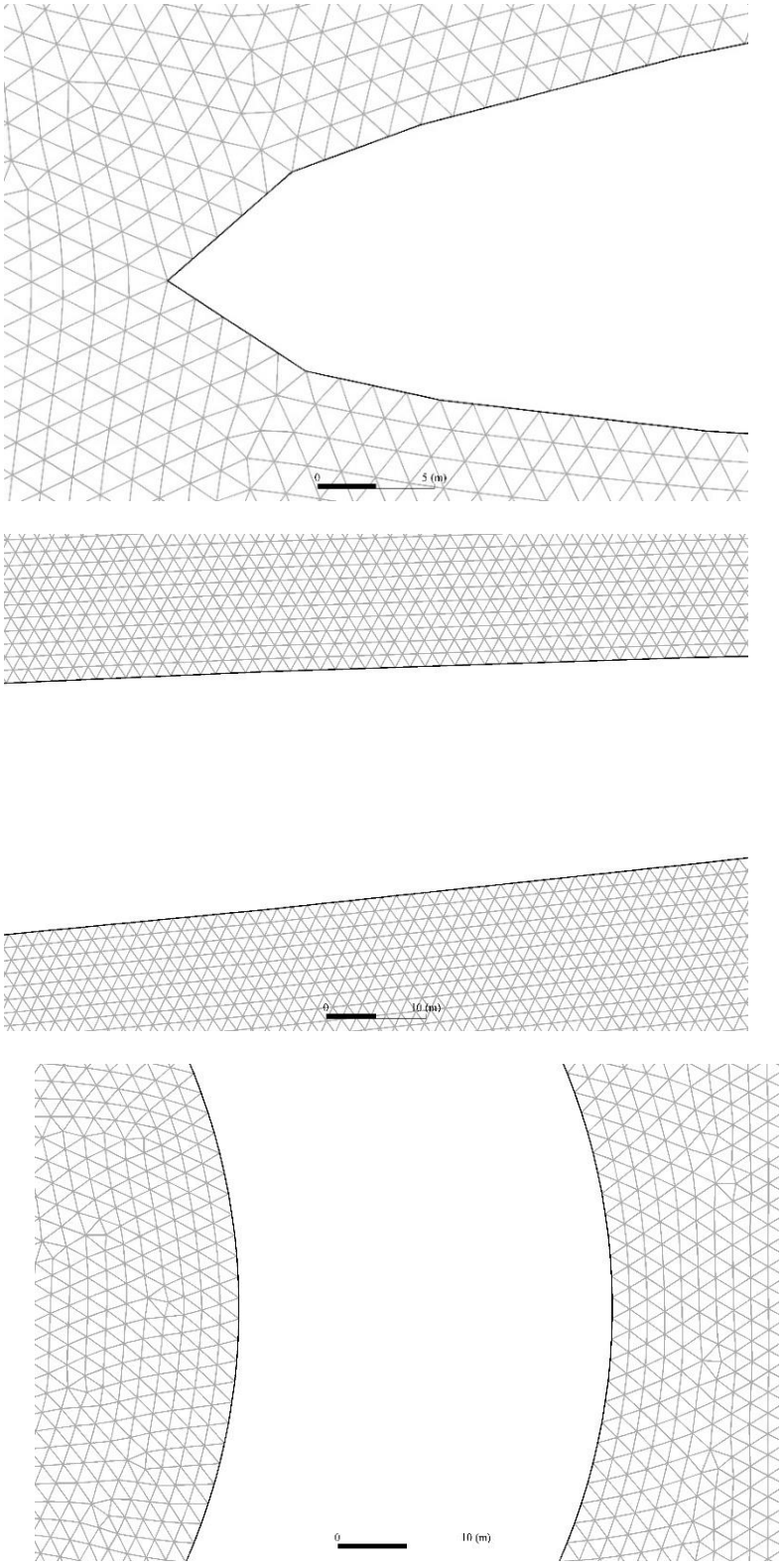

Fig. 3. Computational grid around the shroud's geometry

Table 1. Grid independence for two- and three-dimensional simulations

Model dimension	Grid cell number	The max mean velocity of the domain(m/s)	Max k of domain(m^2/s^2)
2-D	178,390	16.800	30.526
	267,590	18.480	33.579
	401,380	20.328	36.937
	602,100	20.348	36.973
3-D	1,644,000	16.438	19.332
	2,466,000	18.082	21.265
	3,700,000	19.891	23.392
	5,550,000	19.910	23.415

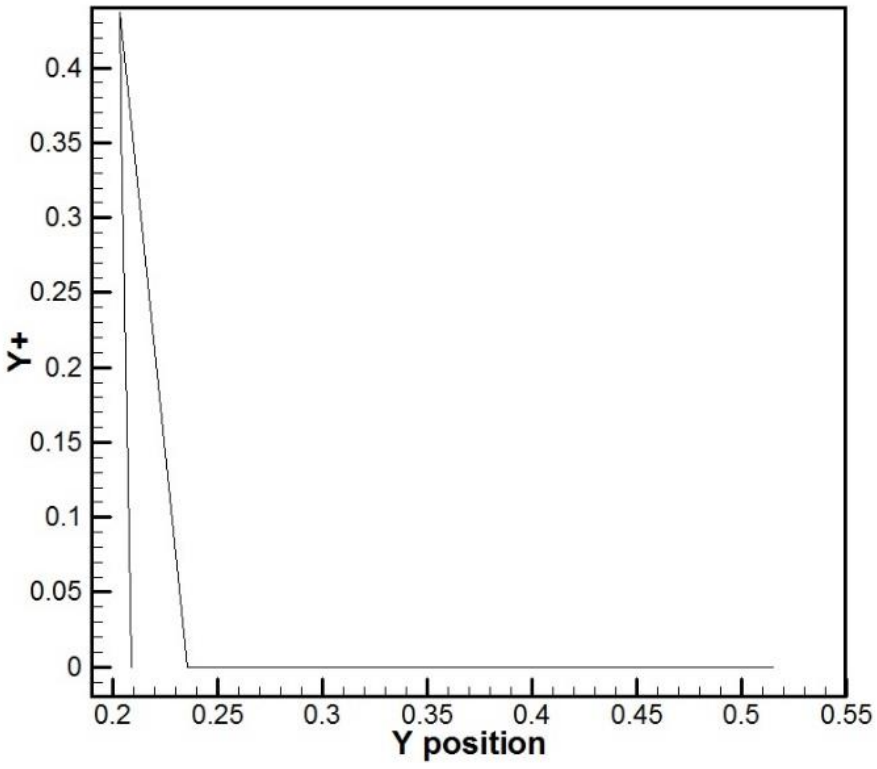

Fig.4 . Y+ diagram near the wind turbine shroud

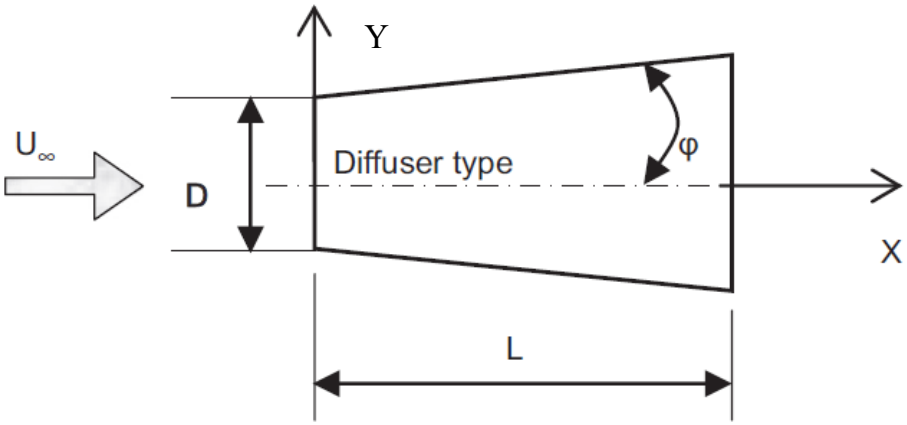

Fig. 5. Diffuser-type shroud in the experiment of Ohya et al[9]

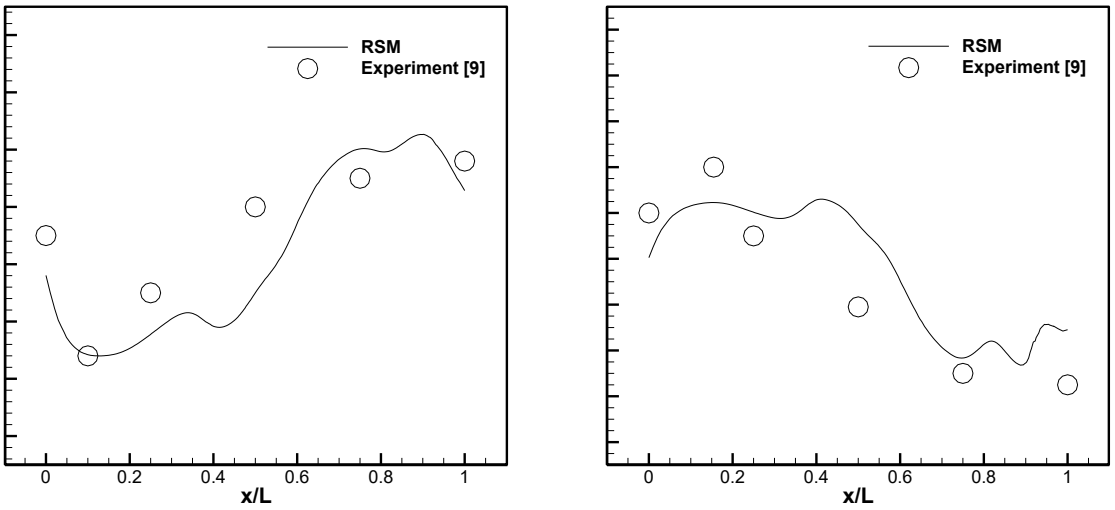

(a) (b)

Fig. 6. The comparison of Cp (a) and velocity (b) inside the diffuser-type shroud between the experiment [9] and the present numerical method

3- The results and discussion

3- 1- Validation

The validity of the proposed numerical method is confirmed by comparing the numerical simulation with the experimental results of Ohya et.al [9]. Ohya et.al conducted a wind tunnel experiment to obtain the pressure coefficient and mean velocity distribution inside three different types of shroud. One of these shrouds is a diffuser type that expands its cross-sectional area from left to right similar to the present study. At the trailing edge of the shroud, a ring-type square flange is installed. The discussed apparatus was then placed in a boundary-layer type wind tunnel. Figure 5 shows the explained diffuser-type shroud.

Ohya's experiment results were reproduced with the proposed numerical method in the present case and these results are compared with corresponding Ohya's results, as shown in Figure 6. The comparison confirmed that there is good agreement between experimental and numerical results.

3- 2- Determining the optimum curvature

In this section, the results for determining the optimum curvature for the installed vertical flange are presented. Various curvatures are examined to find the optimum curvature that produced the maximum mean velocity within the wind turbine shroud. To summarize the results, only five studied cases are presented here. Figure 7 shows the mean velocity profiles at the inlet of straight vertical flange (case 1) and carved flanges their midpoints are displaced to the outlet of the shroud by 1(case 2), 10(case 3), 20(case 4) and 25mm (case 5). The non-dimensional mean velocity magnitude throughout of inlet section of case 4 is higher than the others. This figure expresses that the effect of flange curvature on the shroud's internal flow is to increase the internal flow mean velocity. The inlet flow mean velocity continues to increase until reaching maxima and then due to over bending of the flange, the inlet mean velocity starts to decrease.

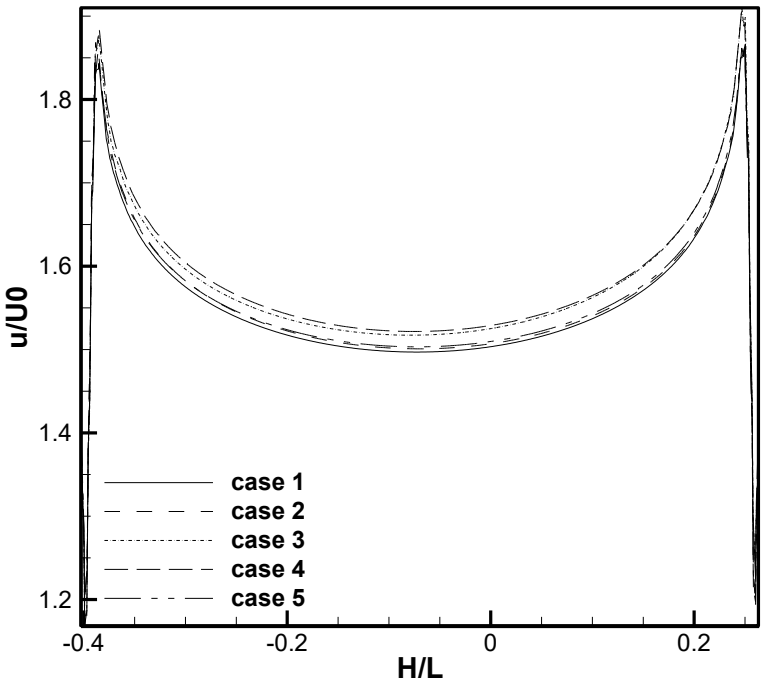

Fig. 7. u/U0 profiles at shroud inlet for cases one to five

Table 2. The values of the average mean and its increased percentage for cases 1-5

Case number	Average mean u/U0	Increase percentage
Case 1	1.558	-
Case 2	1.563	0.320%
Case 3	1.582	1.540%
Case 4	1.587	2.850%
Case 5	1.565	0.449%

Table 2 shows the inlet mean velocity increase percentage from the straight vertical flange model. This must be kept in mind that these models are two-dimensionally simulated and the numerical value may not represent the actual value but the changing trend can be cited in an acceptable way[15].

Figure 9 shows the mean velocity profile behind shroud cases 1 to 5 for five stations. Stations are shown in Figure 8 for clarity. These stations are 206 mm apart from each other.

In Figure 9(a), it is clear that for case 4, severe vortices occur at the end of the shroud and around the flange, resulting from the very intense vortices created by case number 4. These vortices are the same vortices that create a low-pressure area behind the shroud and consequently increase the mass flow rate of air passing through the shroud. The other four geometries, due to the aerodynamic form of their flange, almost have similar and monotonous profile shapes. As the stations get further away, the profiles approach the free flow mean velocity and finally, they become uniform far downstream.

Figure 10(a) shows a summary of the results of the images above. The vertical axis in this image is the ratio of the mean velocity behind the shroud to the wind velocity. Accordingly, the highest value is for case number 4. Also, the increase in entry mean velocity to the shroud can be examined from the perspective of the average turbulence kinetic energy at the stations behind the shroud. The flanges installed at the end of the shroud create vortices that the deformation of the flange towards the optimal point increases the strength of these vortices. Therefore, the amount of turbulence caused by vortices should also be increased. Figure 10(b) shows non-dimensional average kinetic energy at stations behind the shroud. From this figure, by moving towards the flange with the optimal shape, the amount of kinetic energy will also increase and after passing the optimal point, it will start a decreasing process.

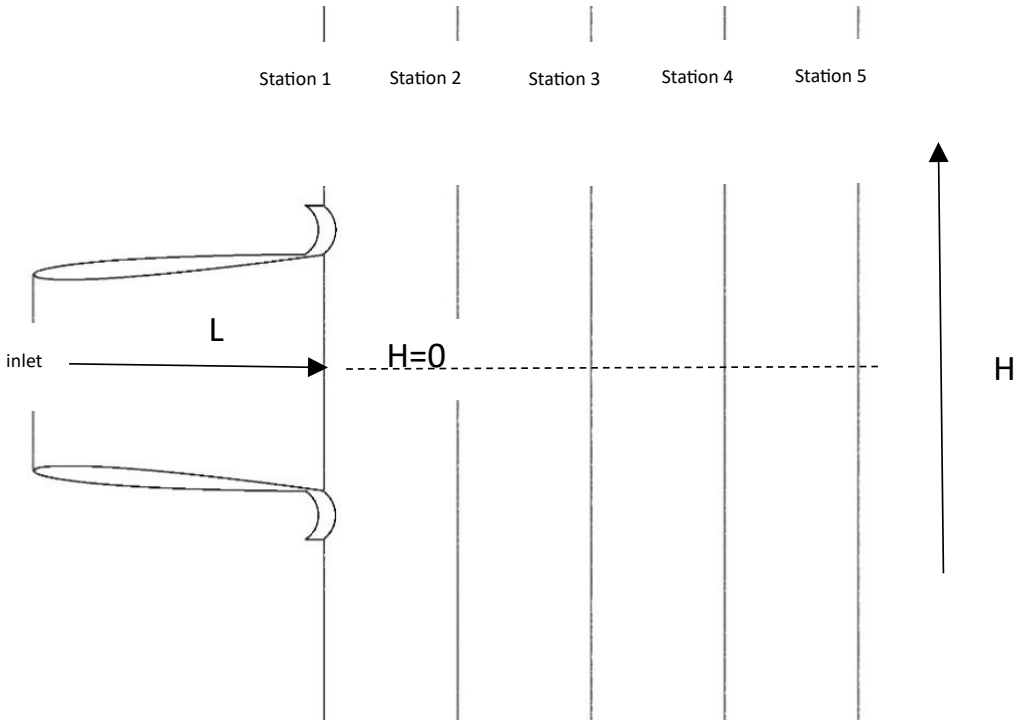

Fig.8 . Computational station locations behind the shroud

3- 3- Comparison of 3D shroud performance with optimal flange and vertical straight flange

In this section, the results obtained from the numerical simulation of a shroud equipped with a flange with an optimal aerodynamic shape and a shroud with a simple straight vertical flange are investigated. The purpose of presenting the results of this simulation is to compare the mean velocity in the part where the turbine is located, called the turbine part, and also to calculate the drag on the whole structure. Therefore, structural engineers can design and select the appropriate materials. The installation location of the turbine has been selected using the results of two-dimensional geometry calculations based on the average flow mean velocity along the shroud. Based on these results, it was found that the location of the turbine should be 118.8 mm away from the inlet of the turbine. Table 3 shows the average mean velocity in this section and its percentage increase for shrouds equipped with optimal aerodynamic and vertical straight flange.

Therefore, based on the above results, it is obtained that the use of optimal flange can increase the airflow rate through the turbine section by 19.930 increase, and this is the first time that the flange deformation to an aerodynamic shape and optimization lead to an increase in mean velocity at the location of the turbine to this value.

3- 4- The conclusion

The present paper deals with the optimization of the aerodynamic shape of the flange connected to the end of the wind turbine shrouds. For this purpose, a large number of aerodynamic sections of the flange have been studied by successively deforming them from the shape of a straight flange. The method was done by moving different midpoints of the simple flange cross-section to create different curves. Then, the rate of increase in mean velocity at the inlet of the shroud has been studied.

The results show that case number 4 will be able to create the maximum mean velocity at the entrance and consequently along the entire length of the shroud.

Based on the results of the three-dimensional simulation, it is concluded that in the turbine section, a mean velocity increase of 20% can be achieved, which is the first time that using an aerodynamic cross-section for flange of shroud and optimizing it has achieved such a great increase in air mean velocity along wind turbine shroud.

To find out the cause of such an increase in mean velocity, a study on turbulent kinetic energy has also been conducted. The vortices caused by the passage of air on the flanges connected to the shroud create a low-pressure area behind the shroud. This low-pressure area creates a higher mean velocity flow in the shroud than in the shrouds without

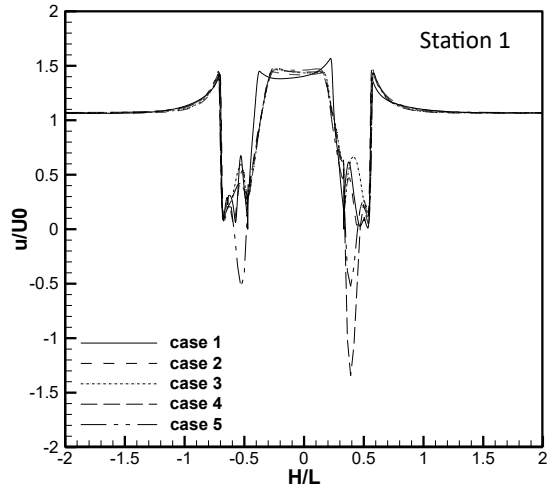

(a)

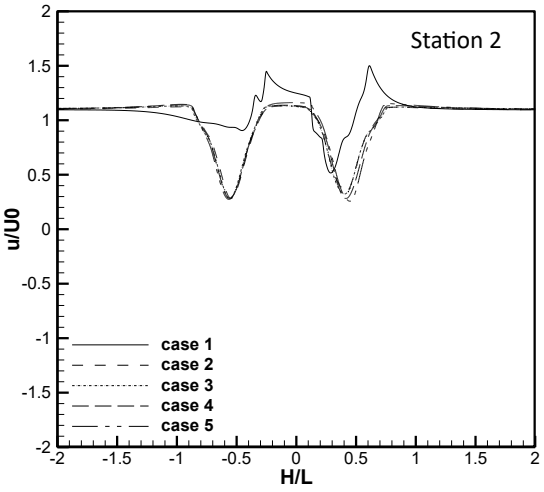

(b)

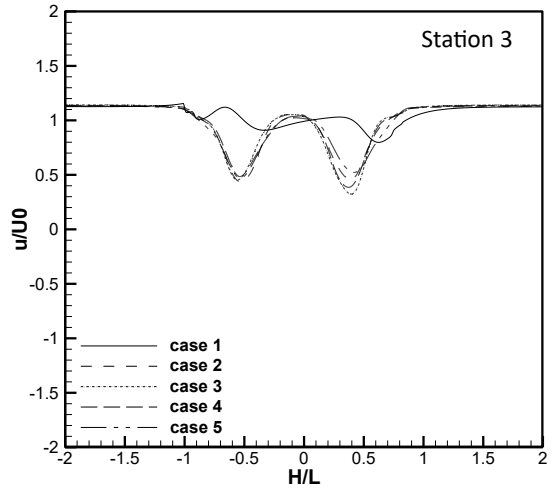

(c)

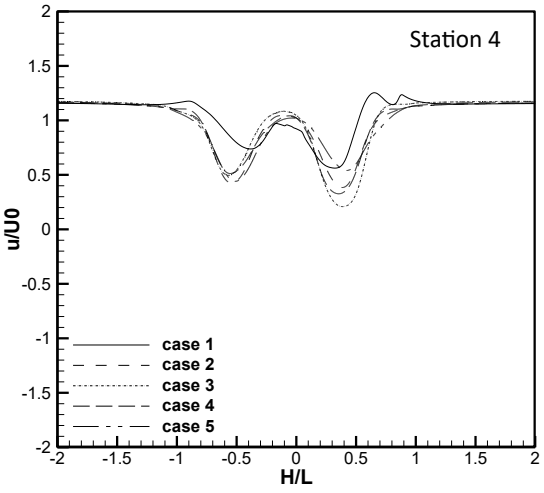

(d)

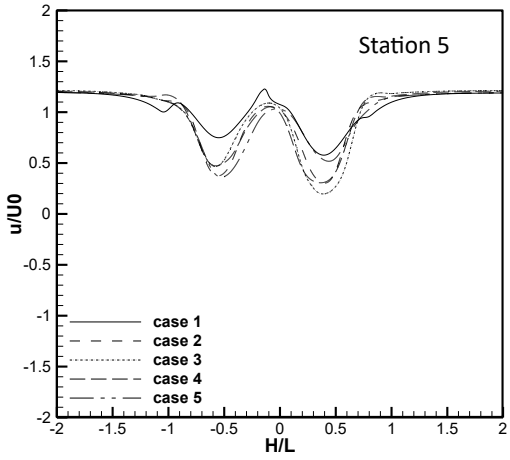

(e)

Fig. 10 . (a) Ratio of average mean velocity to wind velocity (u/U0) behind shroud for cases 1 to 5, (b)Ratio of average turbulence energy to free stream turbulence energy (k/k0) behind shroud for cases 1 to 5

Table 3. The values of average mean velocity and its increased percentage for shroud with simple and optimum curved flanges

Models	Average mean u/U0	Increase percentage
Shroud equipped with a simple vertical flange	15.07687	-
Shroud equipped with an optimal aerodynamic flange	18.081837	19.930

a flange. These vortices increase the turbulence of the areas behind the shroud and increase the turbulent kinetic energy. The results show that the aerodynamic sections continuously increase the kinetic energy of these areas compared to the case using a simple flange until they reach the optimal shape. After passing the optimal point, the amount of kinetic energy in these areas decreases. This confirms past findings.

3- 5- Nomenclature

b_{ij} Reynolds stress anisotropy tensor
C_μ diffusion coefficient
C_1 slow pressure-strain correlation term model coefficient
C_2, C_3, C_4 rapid pressure strain correlation model coefficient
c chord(mm)
D shroud inlet diameter
D_{ij} diffusion term
e_{ij} dissipation rate anisotropy
g gravity constant
H height of virtual stations
h flange height
L shroud length
P pressure
P_{ij} production term
R_{ij} transport of kinematic Reynolds stress
S_{ij} rate of strain
t time
u X velocity component
$\bar{u}$ X average velocity component
u' X velocity fluctuation component
v Y velocity component
$\bar{v}$ Y average velocity component
v' Y velocity fluctuation component
w Z velocity component
$\bar{w}$ Z average velocity component
w' Z velocity fluctuation component
W_{ij} rate of rotation

Greek symbols

δ Displacement of center of flange height
μ dynamic viscosity
ν kinematic viscosity
νt turbulent kinematic viscosity
ε_{ij} dissipation rate tensor
Π_{ij}^R rapid pressure-strain correlation term
Π_{ij}^S slow pressure-strain correlation term
ρ density
σ_k diffusion coefficient
Ω_{ij} rotational term
ω_k rotation vector

References

[1] W. Han, P. Yan, W. Han, Y. He, Design of wind turbines with shroud and lobed ejectors for efficient utilization of low-grade wind energy, Energy, 89 (2015) 687-701.

[2] A. Dilimulati, T. Stathopoulos, M. Paraschivoiu, Wind turbine designs for urban applications: A case study of shrouded diffuser casing for turbines, Journal of Wind Engineering and Industrial Aerodynamics, 175 (2018) 179-192.

[3] M. Shahsavarifard, E.L. Bibeau, Performance characteristics of shrouded horizontal axis hydrokinetic turbines in yawed conditions, Ocean Engineering, 197 (2020) 106916.

[4] A. İlhan, S. TÜMSE, M. TAŞÇI, M. Bilgili, B. ŞAHİN, Particle image velocimetry investigation of the flow for the curved type wind turbine shroud, Journal of Applied Fluid Mechanics, 15(2) (2022).

[5] M. Lipian, I. Dobrev, M. Karczewski, F. Massouh, K. Jozwik, Small wind turbine augmentation: Experimental investigations of shrouded-and twin-rotor wind turbine systems, Energy, 186 (2019) 115855.

[6] M. Lipian, I. Dobrev, F. Massouh, K. Jozwik, Small wind turbine augmentation: Numerical investigations of shrouded-and twin-rotor wind turbines, Energy, 201 (2020) 117588.

[7] Leloudas, G.N. Lygidakis, A.I. Eskantar, I.K. Nikolos, A robust methodology for the design optimization of

diffuser augmented wind turbine shrouds, Renewable Energy, 150 (2020) 722-742.

[8] N.K. Siavash, G. Najafi, T.T. Hashjin, B. Ghobadian, E. Mahmoodi, An innovative variable shroud for micro wind turbines, Renewable Energy, 145 (2020) 1061-1072.

[9] Y. Ohya, T. Karasudani, A. Sakurai, K.-i. Abe, M. Inoue, Development of a shrouded wind turbine with a flanged diffuser, Journal of wind engineering and industrial aerodynamics, 96(5) (2008) 524-539.

[10] L. Gish, A. Carandang, G. Hawbaker, Experimental evaluation of a shrouded horizontal axis hydrokinetic turbine with pre-swirl stators, Ocean Engineering, 204 (2020) 107252.

[11] T. Rezek, R. Camacho, N. Manzanares Filho, E. Limacher, Design of a hydrokinetic turbine diffuser based on optimization and computational fluid dynamics, Applied Ocean Research, 107 (2021) 102484.

[12] T. Rezek, R. Camacho, N. Manzanares Filho, E. Limacher, Design of a hydrokinetic turbine diffuser based on optimization and computational fluid dynamics, Applied Ocean Research, 107 (2021) 102484.

[13] A. Aranake, K. Duraisamy, Aerodynamic optimization of shrouded wind turbines, Wind Energy, 20(5) (2017) 877-889.

[14] M.J. Werle, An enhanced analytical model for airfoil-based shrouded wind turbines, Wind Energy, 23(8) (2020) 1711-1725.

[15] S.N. Leloudas, G.N. Lygidakis, A.I. Eskantar, I.K. Nikolos, A robust methodology for the design optimization of diffuser augmented wind turbine shrouds, Renewable Energy, 150 (2020) 722-742.

[16] M. Yadegari, A. Bak Khoshnevis, A numerical study over the effect of curvature and adverse pressure gradient on development of flow inside gas transmission pipelines, Journal of the Brazilian Society of Mechanical Sciences and Engineering, 42 (2020) 1-15.

HOW TO CITE THIS ARTICLE

A. Niknahad, A. Bak-Khoshnevis, Numerical Investigation Of The Best Wind Turbine Shroud Flange Curvature For Maximum Wind Power Extraction, AUT J. Mech Eng., 7(2) (2023) 185-198.

DOI: 10.22060/AJME.2023.22354.6062